Acceptance-angle effects on the charge transfer and energy-loss cross sections for collisions of C^{4+} with atomic hydrogen

R. Cabrera-Trujillo [1,*] H. Bruhns [2,†] and D. W. Savin [2]

[1]*Instituto de Ciencias Físicas, Universidad Nacional Autónoma de México, Av. Universidad S/N, Col. Chamilpa, Cuernavaca, Morelos, 62210, Mexico*

[2]*Columbia Astrophysics Laboratory, Columbia University, New York, New York 10027-6601, USA*

(Received 5 March 2020; accepted 5 May 2020; published 27 May 2020)

The charge-transfer process for collisions of C^{4+} with atomic hydrogen is studied theoretically and experimentally in this work. Our theoretical study is based on an electron-nuclear dynamics approach applied here for the state-to-state and total contributions to the electron-capture cross sections. Our theoretical results are complemented by experimental measurements of the absolute total cross section for collisions of C^{4+} with atomic hydrogen, which were carried out using an ion-atom merged-beams technique at relative collision energies of 0.122–2.756 keV/u and performed with an improved apparatus at Oak Ridge National Laboratory. We find that the structure observed around a collision energy of 0.5 keV/u in the experimental results is due to the combined contributions of the 3ℓ capture cross sections, the coupling of the electronic and nuclear dynamics, and the acceptance angle in the experimental configuration. We also report the C^{4+} kinetic energy loss and stopping cross section. We find that the C^{4+} gains energy for relative collision energies between 0.1 and 10 keV/u, with a maximum at ∼1 keV/u. Our theoretical study shows that, to compare to the merged-beams experimental results, one has to account for effects produced by the merged path length of the apparatus.

DOI: 10.1103/PhysRevA.101.052708

I. INTRODUCTION

Charge-transfer reactions between positive highly charged ions and atomic hydrogen at low energies are of continued interest in many areas of research. In astrophysics, these reactions can play an important role in determining the ionization and thermal structure of various cosmic plasmas [1]. In nuclear fusion, charge-transfer cross sections are needed for plasma modeling and spectroscopic diagnostics of core, edge, and divertor regions. For example, charge-exchange recombination spectroscopy is the prime diagnostics for measurements of the ion temperature, plasma rotation, and impurity density in the DIII-D tokamak [2]. Furthermore, theoretically, low-energy charge transfer is difficult to calculate due to the quasimolecular states formed during the collision. Benchmark low-energy charge-transfer experiments provide stringent tests of available theories [3].

Charge transfer of C^{4+} with hydrogen, in particular, has been of interest for many years now, with several experimental and theoretical investigations. Phaneuf *et al.* [4] conducted the first measurements in 1982, reporting the total cross section for relative collision energies E, expressed in terms of energy per unit mass, ranging between 0.015 and 0.3877 keV/u, using a laser-produced plasma for the source of C^{4+} ions and a thermal-dissociation atomic hydrogen target. Ćirić *et al.* [5] used photon emission spectroscopy to obtain the absolute cross section for total and state-selective electron capture for C^{4+} ions on atomic hydrogen at collision velocities between 0.1 and 0.5 a.u., equivalent to the range from 0.25 to 6.25 keV/u. Dijkkamp *et al.* [6] performed photon-emission spectroscopy and total cross-section measurements, covering the energy range between 0.83 and 6.6 keV/u using a crossed-beams configuration with a partially dissociated hydrogen beam effused from a radio-frequency discharge source. Hoekstra *et al.* [7] extended the measurements of Dijkkamp with state-selective measurements of the cross section in the energy range between 0.048 and 1.333 keV/u using a deceleration technique. More recently, Bliek *et al.* [8] measured absolute total cross sections for collision energies from 0.0064 to 1.013 keV/u using a previous version of the ion-atom merged-beams apparatus at Oak Ridge National Laboratory (ORNL). The experimental results from Hoekstra *et al.* [7] and Bliek *et al.* [8] showed a structure for relative collision energies around 0.5 keV/u. The study of this structure is the main motivation of this work.

Theoretical charge-exchange calculations for $C^{4+} + H$ were carried out in the 1980's by Fritsch and Lin [9] who used a modified two-center atomic-orbital expansion. Gargaud *et al.* [10,11] used a molecular approach with a three-state model for electron capture into the $3p$ state of C^{3+}. These results agree well with the latest models by Tseng *et al.* [12], Errea *et al.* [13], Vaeck *et al.* [14], and Liu *et al.* [15]. The results of Tseng *et al.* [12] are obtained by using the close-coupling two-center atomic-orbital expansion method with various basis sets. The results of Errea *et al.* [13] are calculated using a molecular basis within a quantum and semiclassical formalism. The results of Vaeck *et al.* [14] employ a full

*Corresponding author: trujillo@icf.unam.mx; On sabbatical leave at the Theoretische Chemie, Physikalisch-Chemisches Institut, Universität Heidelberg, INF 229, 69120 Heidelberg, Germany.

†Present address: Inficon GmbH, Bonner Strasse 498, 50968 Köln, Germany.

 ©2020 American Physical Society

quantum time-dependent method at the complete active space self-consistent field (CASSCF) level with adiabatic potential energy curves, while the results of Liu *et al.* [15] are based on a hyperspherical close-coupling method. The results of Gargaud *et al.*, Tseng *et al.*, Errea *et al.*, and Vaeck *et al*. show moderately good agreement with the state-selective measurements from Hoekstra *et al.*. However, below about 1 keV/u all these theories predict a higher total cross section than that measured by Phaneuf *et al.* [4], Dijkkamp *et al.* [6], and Bliek *et al.* [8]; and none of them display the experimental structure around 0.5 keV/u mentioned previously.

In this article, we present a theoretical study based on a solution to the time-dependent Schrödinger equation, with the inclusion of nonadiabatic electron-nuclear dynamics, to calculate the total and 3ℓ-state-resolved electron-capture cross section to understand and elucidate the origin of the observed structure near $E \approx 0.5$ keV/u. We complement our theoretical study by new experimental data obtained using the ion-atom merged-beams apparatus at ORNL. The apparatus has undergone significant modifications [16] since the measurements of Bliek *et al.* [8], so that our results here can be considered as another independent measurement.

The paper is organized as follows. In Sec. II, we summarize our theoretical approach to obtain the state and total electron-capture cross sections, as well as the projectile kinetic energy loss or gain during the collision. Section III gives a brief overview of our measurement technique with particular emphasis on the improvements in the angular collection of the present apparatus and a discussion of the contribution to the cross section due to the small metastables fraction expected in the C^{4+} ion beam. Our results are discussed in Sec. IV starting with the discussion of the capture probability and the electron-capture cross section. A discussion of the acceptance angle is then presented followed by the projectile energy loss and stopping cross section. Finally, in Sec. V, we provide our conclusions. Atomic units (a.u.) are used through this work, except where physical units are explicitly stated.

II. THEORETICAL APPROACH

A. Collision frames

Our theoretical study is carried out in a frame where the target is initially at rest, which we call the target-rest frame. However, in the merged-beams experiment, both the projectile and target are moving, which we call the target-moving frame. From collision theory [3], the projectile-target system has a total kinetic energy given by the sum of the center-of-mass kinetic energy and the relative collision kinetic energy. The kinetic energy of the center of mass is given by $E_{\rm cm} = m_T \mathbf{v}_{\rm cm}^2/2$ where $m_T = m_1 + m_2$ is the total mass and $\mathbf{v}_{\rm cm} = (m_1\mathbf{v}_1 + m_2\mathbf{v}_2)/m_T$. Here, the index 1 stands for the projectile and 2 for the target in the laboratory frame and $E_{\rm cm}$ is a constant of motion of the system. The relative collision energy is given by $E_r = \mu v_r^2/2$ where $\mu = m_1 m_2/m_T$ is the reduced mass and $\mathbf{v}_r = \mathbf{v}_2 - \mathbf{v}_1$ is the projectile-target relative velocity. The target-rest frame of the theoretical study and the target-moving frame of the experimental measurements differ only by the velocity of the target. Transforming between frames shifts v_1 and v_2 by the same value, yielding the same $v_{\rm r}$ independent of frame choice. Thus the relative energy is the energy that characterizes the collision in both frames. As is customary in collision theory, we shall express our results in terms of the energy per unit mass, i.e., $E = E_r/\mu = v_r^2/2$.

B. Electron-nuclear dynamics

For the study of the electron-capture process, we use a nonadiabatic approach that takes into account the electronic and nuclear coupling within the time-dependent variational principle (TDVP) to solve the time-dependent Schrödinger equation. This method is called electron-nuclear dynamics (END) and it has the advantage that it is not restricted to straight-line trajectories. As the details of the END method have been reported elsewhere [17], we present here only a brief summary of the theory.

Application of the variational principle to the quantum action yields the time-dependent Schrödinger equation when variations of the wave function over the state space are performed. We use a parametrization of the wave function in a coherent-state manifold, which leads to a system of Hamilton's equations of motion [17]. The simplest implementation of the END approach employs a single spin-unrestricted electronic determinant written in terms of nonorthogonal spin orbitals whose **c** coefficients describe the electron dynamics. These electronic molecular orbitals are, in turn, expressed in terms of a basis of augmented Gaussian atomic-type orbitals of rank K with complex coefficients. The Gaussian-type orbitals are centered on the average positions **R** of the participating atomic nuclei, which are moving with momentum **P**. This representation takes into account the momentum of the electrons explicitly by means of electron translation factors [17]. The nuclear part of the wave function is represented by localized Gaussian functions, which in the narrow wave-packet limit become classical trajectories coupled to the electronic degrees of freedom. Application of the TDVP yields the dynamical equations, which include the nonadiabatic coupling terms between the electrons and nuclei. Solving the set of equations for {**c**, **R**, **P**} as a function of time generates the evolving molecular state that describes the processes that take place during the collision. This scheme has been implemented in the ENDyne program package [18].

Analysis of the collision requires the specification of initial conditions of the system under consideration. The initial C^{4+} projectile velocity is set parallel to the z axis and directed towards the stationary H target with an impact parameter b along the xy plane. The target H atom has been initially placed at the origin of a Cartesian laboratory coordinate system. In these calculations the projectile is initially set at a distance of 50 a.u. from the target and in the self-consistent electronic ground state $C^{4+}(1s^2)$. The impact parameter b is chosen in the range 0–20 a.u. in steps of 0.1 from 0.0 to 4.0, in steps of 0.2 from 4.0 to 6.0, in steps of 0.4 from 6 to 10, and in steps of 1.0 from 10 to 20 a.u. This gives a total of 70 fully dynamical trajectories for each projectile energy.

The electronic basis set used for the H atom is the aug-cc-pVDZ basis set of Dunning [19] consisting of $[5s3p/2s2p]$ and expanded by two s and p even-tempered [20,21] diffuse orbitals to account for polarization effects on the atomic target. For C^{4+}, we use the aug-cc-pVTZ electronic basis set

consisting of $[10s4p2d/5s3p2d]$. These bases sets provide a good compromise between computational time and a proper description of the excited states of the system.

Once the wave function is determined at the end of the time evolution, the electron-capture probability, as a function of the impact parameter b, is obtained by a projection of the projectile nth state as

$$P_n(b, E_r) = |\langle \psi_n | \Phi(b, E_r) \rangle|^2 , \tag{1}$$

where ψ_n is the final capture state of the projectile and Φ is the final evolved molecular wave function. The total electron capture probability, $P(b, E_r)$, is the sum over all the state contributions.

We define a total electron-capture cross section as a function of the allowed scattering angles $\sigma(\Omega_a)$, i.e., for projectiles which are scattered within the solid angle Ω_a, as

$$\sigma = \int_{\Omega \in \Omega_a} \frac{d\sigma}{d\Omega} d\Omega . \tag{2}$$

Here we perform the scattering analysis using a classical impact-parameter description. Then the deflection function (the scattering angle as a function of the impact parameter), $\theta = \Theta(b)$, gives the classical differential cross-section

$$\frac{d\sigma(E_r)}{d\Omega} = P(b, E_r) \frac{b}{\sin(\theta)} \left| \frac{db}{d\theta} \right| . \tag{3}$$

Then the classical total charge-exchange cross section is

$$\sigma(E_r) = 2\pi \int_{[b]_a} bP(b, E_r) db , \tag{4}$$

where $[b]_a$ is the set of impact parameters within an acceptance angle θ_a, the maximum acceptance angle of the scattering problem, relative to the center-of-mass velocity. Here P denotes either the total or the nth state electron-capture probability. Thus, a correct description of the scattering trajectory is required. For further details of the implementation of the acceptance angle, see Ref. [22]

The END approach provides the final momentum of the nuclei. In the target-rest frame, we define the kinetic energy loss for the projectile as $\Delta\mathcal{E}(b, E_r) = E_p^f(b, E_r) - E_p^i$, where E_p^f is the projectile final kinetic energy and E_p^i the projectile initial kinetic energy. From energy conservation, we have that

$$\begin{aligned} -\left(E_p^f - E_p^i\right) &= \left(E_{p,e}^f - E_{p,e}^i\right) + \left(E_{t,e}^f - E_{t,e}^i\right) \\ &\quad + \left(E_t^f - E_t^i\right) \equiv -\Delta\mathcal{E} , \end{aligned} \tag{5}$$

where the superscripts i or f stands for initial or final, while the subscript p or t stands for projectile or target. Here, the subindex e indicates the electronic energy in the projectile or target. This means that for a projectile energy loss $\Delta\mathcal{E} < 0$, there is an energy gain in the target nuclear energy and in the excitation energy of the system. Thus, the stopping cross section, that is, the cross section for the projectile kinetic energy loss is given by

$$S(E_r) = -2\pi \int_0^\infty b\, \Delta\mathcal{E}(b, E_r)\, db . \tag{6}$$

This is a measure of nonadiabatic effects that take place during the collision as the projectile kinetic energy is modified by the momentum and charge transferred during the collision. The negative sign is to assure that S is positive for energy loss [23]. With this, the electronic stopping cross section is given as

$$S_e(E_r) = 2\pi \int_0^\infty b\, \Delta\mathcal{E}_e(b, E_r)\, db , \tag{7}$$

and the nuclear stopping cross section as

$$S_n(E_r) = 2\pi \int_0^\infty b\, \Delta\mathcal{E}_n(b, E_r)\, db . \tag{8}$$

Here, $\Delta\mathcal{E}_e = (E_{p,e}^f - E_{p,e}^i) + (E_{t,e}^f - E_{t,e}^i)$ is the energy loss of the projectile that goes into electronic excitations and ionization in the projectile-target system and $\Delta\mathcal{E}_n = (E_t^f - E_t^i)$ is the target recoil kinetic energy (target displacement). These are positive quantities when the transferred energy is gained by the target through target excitations and target nuclei recoil.

III. EXPERIMENTAL PROCEDURE

The ion-atom merged-beams technique is well established in the literature [24,25], and so we will only briefly describe the experiment here. A beam of ground-state atomic hydrogen is produced by the photodetaching part of an 8-keV H^- beam that passes through a Nd:YAG laser cavity. The remaining H^- beam is subsequently electrostatically removed from the atomic H beam. Unwanted electronically excited hydrogen atoms, produced through collisional stripping of the H^- beam on the residual gas in the vacuum chamber, are almost completely removed by passing the beam through an electric field ionizer with a field strength of 30 kV/cm. The remaining contribution of non-laser-produced H atoms to the measured cross section (usually on the order of up to 5%) is determined and corrected for by repeating every measurement with the laser beam turned off. A permanent magnet Electron Cyclotron Resonance (ECR) source on a high voltage platform is used to produce a C^{4+} ion beam with energies between 121 and 240 keV.

The ion and neutral beams are merged by means of an electrostatic spherical deflector with a 1-cm diameter circular hole for the neutral beam to pass through. The two beams run collinear for a distance of 32.5 cm and undergo the charge transfer reaction

$$C^{4+} + H(1s) \rightarrow C^{3+} + H^+ . \tag{9}$$

At the end of the merge path, the C^{4+} and C^{3+} ions as well as the signal-protons are magnetically dispersed, with both the C^{4+} and C^{3+} ions being collected in the same Faraday cup. The neutral beam is monitored by measuring the secondary-electron emission from a stainless steel plate. The neutral detector is calibrated *in situ* [25].

The signal protons are electrostatically deflected out of the dispersion plane and directed into a channel electron multiplier (CEM) detector using electrostatic steerers and lenses to collect the signal.

The actual merge path is terminated just before the dispersing magnet by an Einzel lens, which is part of the signal-proton focusing system: any protons created within the electrostatic potential of this Einzel lens have a different kinetic energy than the signal protons from within the potential-free merge path. Thus, they are not within the accepted phase

space of the subsequent ion optical elements, and are therefore not detected.

The ORNL merged-beams apparatus has changed significantly [16] since the measurements by Bliek *et al.* [8]. The ion beam is now produced by a permanent-magnet ECR ion source mounted on a high voltage platform. With the old setup, Bliek *et al.* were unable to generate ion beams of sufficiently high energy to match the velocity of the H beam. Thus to achieve low ion-atom collision energies they had to use D beams, which travel more slowly than H for the same neutral beam energy. The new setup is able to merge higher kinetic energy ion beams than previously (transporting now up to $q \times 150$ keV) such that the ion velocity can match that of the atomic hydrogen beam. This allows us to perform the entire experiment with H.

The machine also features a shorter merge path and improvements to the beam-beams overlap measurement system [26]. Low-energy charge transfer is expected to lead to large angular scattering [27] because of the Coulomb repulsion of the reaction products. This angular scatter becomes even more demanding for signal collection when the reaction is exoergic and leads to an additional kinetic energy release in the center of mass. In the energy range studied, the predicted importance of rotational coupling [28] may further amplify the angular scatter. Due to the shorter merge path and the higher velocity beams, the angular collection in the center-of-mass frame has significantly increased for the upgraded apparatus, as is discussed below.

Since the merged beams travel at keV energies in the laboratory frame, the angular spreads of the two reaction products are strongly compressed in the forward direction. As derived in Ref. [24], the scattering angle in the laboratory $\theta_{\rm lab}$ measured relative to $\mathbf{v}_{\rm cm}$ is related to the scattering angle in the center-of-mass frame $\theta_{\rm cm}$ by

$$\tan\theta_{\rm lab} = \frac{(\mu/m_1)v_r^f \sin\theta_{\rm cm}}{v_{\rm cm} + (\mu/m_1)v_r^f \cos\theta_{\rm cm}}, \tag{10}$$

where $v_{\rm cm} = |\mathbf{v}_{\rm cm}|$, v_r^f is the final relative velocity after the collision, m_1 is the mass of the faster collision partner, and μ is the reduced mass of the collision system. If m_1 is the slower collision partner, the plus sign in the denominator needs to be replaced by a minus sign.

The first version of the ORNL ion-atom merged-beams apparatus [24] lacked sufficient angular collection to collect all the beam-beam signal throughout $E = 0.001$–1 keV/u range. Assuming the structure observed around relative collision energies of 0.5 keV/u in the measurement by Bliek *et al.* [8], who measured with a signal acceptance angle in the laboratory frame (i.e., the target-moving frame) of 2.3°, is due to such signal collection issues, then a change in the angular acceptance of the apparatus could change the shape of the structure, or make it disappear. The present ORNL merged-beams apparatus has an improved angular acceptance of 3.5° in the laboratory frame, which corresponds to an angular collection of 7° at 3 keV/u to 37° at 0.15 keV/u in the center of mass.

Although the previous apparatus acceptance was sufficient for the expected angular scatter as calculated by Olson and Kimura [27] using a "half-Coulomb" Rutherford scattering model, their work did not take into account rotational coupling. For example, a laboratory angular collection of 2.3° is not sufficient to collect the signal for $He^{2+} + H$ for $E \lesssim 0.8$ keV/u where rotational coupling significantly increases angular scattering above the half-Coulomb estimate [29].

For the measurements performed here, the fraction of C^{4+} beam in electronically excited metastable states was not determined. As was estimated by Bliek *et al.* [8] using a multichannel Landau-Zener calculation, the cross section for capture by a ground-state $C^{4+}(1s^2)$ ion is larger by ∼40% than capture by an ion with an excited core, i.e., a $1s2s(^1S)$ or $1s2s(^3S)$ C^{4+}. This enhancement for capture into the ground state is almost constant for collision energies above 0.1 keV/u [8]. The $1s2s(^1S)$ excited state has a lifetime of only 3.3 μs [30], as compared to the tens of μs flight time from the ECR source to the merge section and can thus be neglected.

The fraction of metastable C^{4+} ions in the long-lived $1s2s(^3S)$ term in beams extracted from ECR ion sources has been measured by several different groups [7,8,31]. In each case the fraction of metastable ions in the beam was determined to be (5 ± 2)%. We assume the same metastable content for our ion beam. For this metastable fraction, our results have to be corrected by 0.05×0.4–0.02, or (2 ± 1)% toward higher cross sections.

Finally, because the metastable content of the ion beam is expected to be small, and because the metastable C^{4+} ions are predicted to have generally lower cross sections for charge transfer than ground state ions, then any structure in the cross section exclusively due to metastable ions is suppressed. In particular, if at a certain E_r there were no charge transfer with metastable ions at all, the maximum decrease of the measured cross section would be 2% (the metastable contribution to the cross section). Thus, it is difficult to attribute any significant structure seen in the data to an incorrect estimate of the metastable content in our ion beam.

To obtain the total absolute error, several systematic uncertainties have to be taken into account [24]. The systematic contribution to the total uncertainty is estimated to be 12% at a 90% confidence level, which is mostly due to the beams overlap and the atomic H particle current determination. The total experimental uncertainty is calculated by adding the statistical and systematic uncertainties in quadrature.

IV. RESULTS AND DISCUSSION

A. Electron-capture probability

In Fig. 1, we show the impact-parameter-weighted total electron-capture probability, $bP(b)$, as a function of the impact parameter for several collision energies (color lines). In the same figure, we show the projectile energy loss weighted by the impact parameter $b\Delta\mathcal{E}$ whose discussion is left for Sec. IV E. We find that the largest contribution to the total electron-capture cross section is for $E \approx 0.3$ keV/u and impact parameters of around $5 < b < 8$ a.u., which is responsible for the maximum observed in the total electron-capture cross section. For higher collision energies, the maximum contribution shifts towards lower impact parameters, around $4 < b < 6$ a.u. Also, at high collision energies, we observe fewer oscillations in the electron-capture process, but as E is reduced, the number of oscillations increases, reaching a

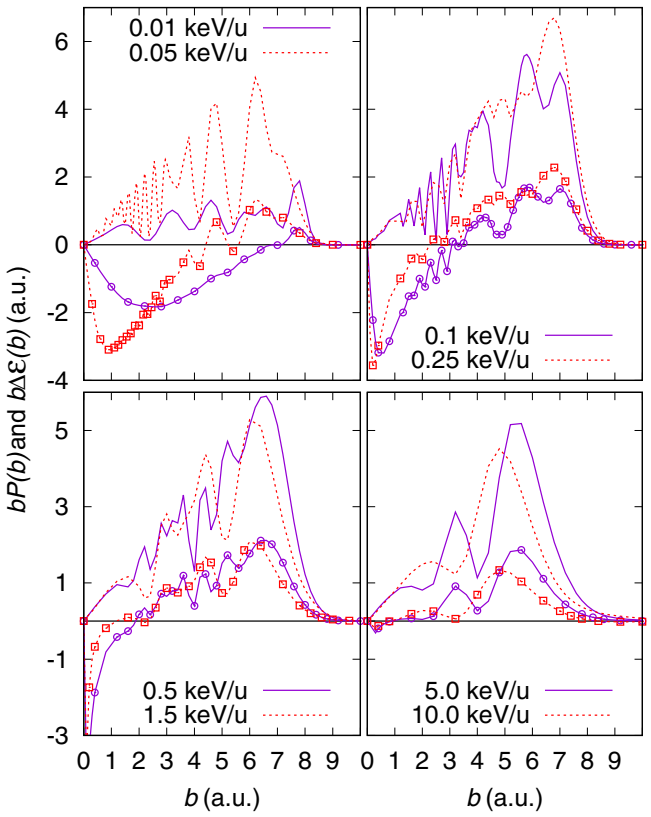

FIG. 1. Impact-parameter-weighted total electron-capture probability $bP(b)$(color lines) and projectile kinetic energy loss weighted by the impact parameter $b\Delta\mathcal{E}$ (same color lines with open symbols) as a function of the impact parameter b for several relative collision energies for C^{4+} colliding with atomic H, as obtained with the END approach. See text for discussion.

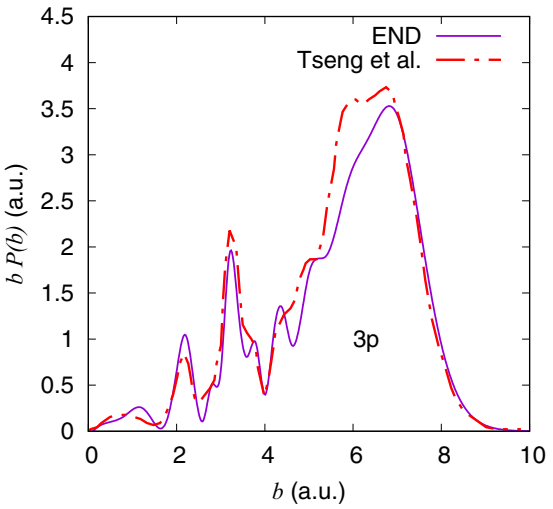

FIG. 2. Electron-capture probability, weighted by the impact parameter, for capture into the $3p$ state of the projectile, as a function of the impact parameter, for C^{4+} colliding with atomic H for a relative collision energy of 0.5 keV/u. We compare the $3p$-state electron-capture results to those obtained by Tseng *et al.* (red dot-dashed line) [12] showing very good agreement between both approaches.

highly oscillatory behavior for $E = 0.08$ keV/u and impact parameters $1 < b < 3$ a.u. This oscillatory behavior is the result of Stückelberg interference effects between the entrance and exit capture channel [29]. For lower values of E, Stückelberg oscillations start to diminish as well as the contribution to the electron-capture cross section. We find that for $b > 8$ a.u. the electron capture is suppressed for all values of E_r as at larger distances the projectile-target interaction is small. Also, there is only a very small contribution from the rotational region, i.e., $b < 1.5$ a.u., the region where the rotational coupling dominates. Although the rotational coupling produces capture probabilities reaching almost unity, the impact parameter weight makes its contribution to the cross section small in this region. Thus, we find that the largest electron-capture probability contribution to the cross section comes from the radial region of the collision, $2 < b < 8$ a.u..

To validate the electron-capture probabilities, we show in Fig. 2 the impact-parameter dependence of the electron-capture cross section for the $3p$-state contribution when C^{4+} collides with atomic hydrogen for $E = 0.5$ keV/u, and compare to the theoretical results of Tseng *et al.* [12]. We observe that the END and Tseng *et al.* results agree very well for all the impact parameters, with the exception of b around 6 a.u. where END shows a lower contribution. However, the agreement in the oscillation for the electron-capture probability for $b < 5$ a.u., which we attribute to the Stückelberg interference process in the electron-capture dynamic [29], is very good for both approaches. In this case, the largest contribution to the electron-capture cross section occurs for the region $b \sim 7$ a.u., forming C^{3+} with an empty $n = 2$ shell.

B. State-to-state capture cross section

In Fig. 3, we show the 3ℓ-state contribution to the electron-capture cross section. In the same figure, we compare to the theoretical results of Gargaud *et al.* (blue double-dot-dashed line) [11], Tseng *et al.* (red dot-dashed line) [12], Errea *et al.* (green long-dashed line) [13,32], Vaeck *et al.* (black short-dashed line) [14], and Liu *et al.* (orange triple-dash line) [15]. We also compare to the experimental data of Dijkkamp *et al.* (▽) [6] and Hoekstra *et al.* (○) [7]. We notice that the END results agree reasonably well with the experimental data. From these results, we note that the $3l$ electron-capture cross sections are, in part, responsible for the structure observed at $E = 0.5$ keV/u. The sum of the $3s$, $3p$, and $3d$ excited states capture cross section provides the shape of the overall total electron-capture cross section at these intermediate values of E. For the capture into the $3d$ state, the experimental data drops off faster than our END results for values of $E \lesssim 0.1$ keV/u. Our results show a large contribution between 0.01 and 0.07 keV/u, but agree fairly well with the theoretical data of Errea *et al.*, Vaeck *et al.*, and Liu *et al.* and with the experimentally observed minimum at 0.1 keV/u.

Also, we note that for values of $E > 2$ keV/u, the END results show a lower contribution for the state-to-state cross section in the $3d$ state. The reason is the opening of the ionization channel for atomic H in a collision with C^{4+}, which the END basis set is not able to account for properly. As shown by Bohr [23], the ionization channel opens for a hydrogen atom for a relative collision velocity of $v_r = v_0/Z_p$ with v_0 being the Bohr velocity and Z_p the projectile effective charge.

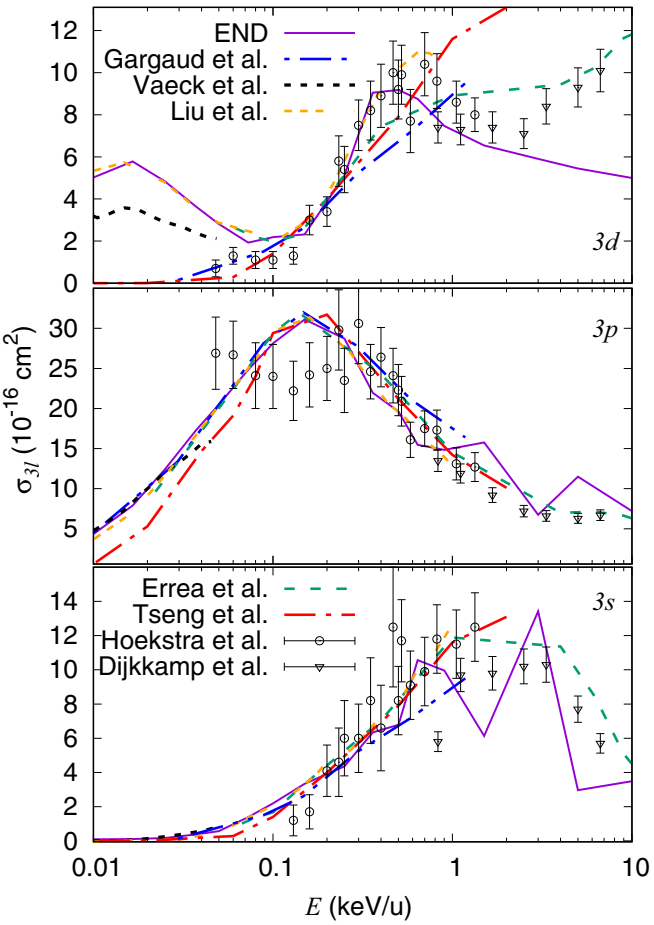

FIG. 3. END theoretical charge-transfer cross section results for the 3ℓ states (purple solid line) shown together with the results of Gargaud *et al.* (blue double-dot-dashed line) [11], Tseng *et al.* (red dot-dashed line) [12], Errea *et al.* (green long-dashed line) [13,32], Vaeck *et al.* (black short-dashed line) [14], and Liu *et al.* (orange triple-dash line) [15], as well as the available experimental data from Dijkkamp *et al.* (▽) [6] and Hoekstra *et al.* (○) [7] as a function of the relative collision energy per unit mass, E.

Assuming, in our case, that $Z_p = q = 4$ then $v_r = v_0/4$, which corresponds to $E = 1.5$ keV/u. Thus, ionization of hydrogen when colliding with a highly charged C^{4+} starts to influence the electron capture for $E \gtrsim 2$ keV/u. Hence, due to the lack of continuum states in the END approach, our results start to have a different behavior as compared to the experimental data for $E \gtrsim 2$ keV/u.

In Table I, we provide our theoretical results for the total and $n = 3$ cross section as obtained with the END approach for reference.

C. Total electron-capture cross section

Figure 4 shows our theoretical (purple solid line) and experimental (black filled squares) results for the total electron-capture cross section, as well as the theoretical results of Fritsch *et al.* (brown long-dashed line) [9], Gargaud *et al.* (blue double-dot-dashed line) [11], Tseng *et al.* (red dot-dashed line) [12], Errea *et al.* (green long-dashed line) [13,32], Vaeck *et al.* (black short-dashed line) [14], and Liu *et al.* (orange triple-dash line) [15]. All the theoretical works give similar results, without any indication of structure, for $E = 0.01$ and 10 keV/u. We also compare to the experimental results of Phaneuf *et al.* (□) [4], Ćirić *et al.* (△) [5], Dijkkamp *et al.* (▽) [6], Hoekstra *et al.* (○) [7], Bliek *et al.* (◊) [8], and our present results.

For low E, the experimental results of Phaneuf *et al.* [4] are in better agreement with our theoretical results for $E \lesssim$

TABLE I. Theoretical total and $n = 3$ electron-capture cross sections for C^{4+} colliding with H for $E = 0.01$–10 keV/u as obtained with our END approach.

Collision energy (keV/u)	Total σ	$n\ell$ $3s$	$3p$	$3d$
	(10^{-16} cm^2)			
0.01	10.18	0.09	4.35	5.02
0.0165	14.88	0.11	7.88	5.78
0.025	18.88	0.17	12.40	4.84
0.0375	23.51	0.38	17.34	3.62
0.05	26.71	0.57	20.49	2.81
0.073	31.26	1.38	24.78	1.93
0.10	35.94	2.19	28.14	2.18
0.15	40.61	3.34	31.09	2.32
0.25	41.98	4.34	28.71	5.12
0.50	39.56	6.79	19.62	9.18
0.90	37.08	9.96	14.83	7.46
1.50	34.45	10.23	11.68	6.54
3.00	31.13	13.42	6.75	5.91
5.00	28.86	7.84	6.63	5.45
10.00	26.14	3.50	7.21	5.00

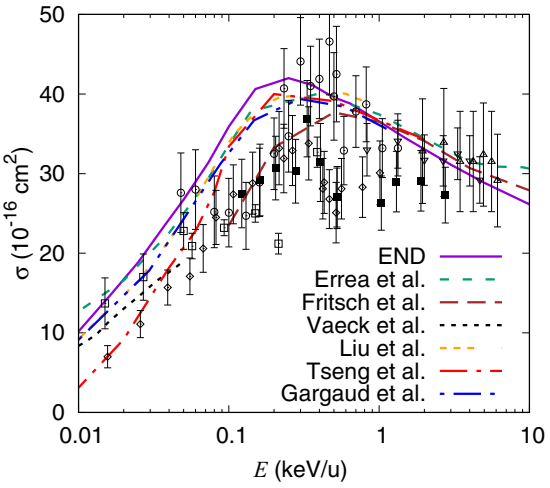

FIG. 4. Present experimental (■) and theoretical END (purple solid line) total electron-capture cross-section results shown together with other experimental data from: Phaneuf *et al.* (□) [4]; Ćirić *et al.* (△) [5]; Dijkkamp *et al.* ▽ [6]; Hoekstra *et al.* (○) [7]; and Bliek *et al.* (◊) [8]. Also shown are the theoretical data by Fritsch *et al.* (brown long-dashed line) [9], Gargaud *et al.* (blue double-dot-dashed line) [11], Tseng *et al.* (red dot-dashed line) [12], Errea *et al.* (green long-dashed line) [13,32], Vaeck *et al.* (black short-dashed line) [14], and Liu *et al.* (orange triple-dash line) [15].

TABLE II. Measured total electron-capture cross sections for C^{4+} on H, including correction for metastables in the ion beam. All measurements were performed with an 8-keV atomic hydrogen beam and an acceptance angle of 3.5° in the laboratory frame.

Collision energy (eV/u)	Cross section (10^{-16} cm^2)	Uncertainties Statistical (10^{-16} cm^2)	Uncertainties Total (10^{-16} cm^2)
122	27.5	2.7	4.3
161	29.2	2.9	4.5
205	30.7	1.5	4.0
278	30.3	1.8	4.0
332	36.9	1.8	4.8
407	31.4	3.1	4.9
524	27.0	1.9	3.7
525	27.0	2.1	3.9
1033	26.3	1.3	3.4
1304	29.0	1.4	3.8
1895	29.1	1.4	3.8
2756	27.3	1.3	3.5

0.06 keV/u than the other experimental data. We observe that the Hoekstra *et al.* [7] results are in very good agreement with our theoretical data for $E \gtrsim 0.2$ keV/u. In general, though, we find that all the theoretical results (including our END data), lie higher than the experimental data of Bliek *et al.* [8] and our present experimental data. None of the calculations show the structure seen above 0.5 keV/u in these two experimental data sets. Interestingly, we find that the data of Hoekstra *et al.* shows a similar structure in the total cross section around 500 eV/u.

In Table II, we provide our measured total electron-capture cross sections for C^{4+} on H versus E for reference purposes, as obtained for an acceptance angle of 3.5° in the laboratory frame (i.e., the target-moving frame).

D. Acceptance-angle electron-capture cross section

To understand the origin of the structure observed in the experimental data, we analyze the scattering angles of the projectile and target. As the H^+ ion is used to determine the charge-transfer cross section in the experiment, we calculate the H^+ scattering angle within our END approach. These results are shown in Fig. 5. We observe that the largest scattering angle in the laboratory frame is close to 16° for 1.5 keV/u and impact parameters between $0 < b < 1$ a.u. In the same figure, the experimental value of the acceptance angle used in our experiment, $\theta_a = 3.5°$, is shown by a horizontal line. Falling above this line indicates the region of impact parameter and scattering angles for H^+ ions that are not collected in the experimental measurements for the charge-transfer process. Below this line determines the set of $[b]_a$ of Eq. (4).

In Fig. 6, we show the integrated charge-transfer cross section, as a function of the acceptance angle, for $E = 0.01$, 0.05, 0.1, 0.25, 0.5, 0.65, 0.9, and 1.5 keV/u as obtained from the END approach. We observe that for $E \gtrsim 0.25$ keV/u, the total charge-transfer cross section basically reaches its total value for an acceptance angle around 2°. However, for $E \lesssim 0.05$ keV/u an acceptance angle of 2.3° or 3.5° makes a significant different contribution to the charge-transfer cross section (shown by vertical lines). For lower values of E, a larger acceptance angle is required to account for the whole contribution to the charge-transfer cross section. Thus, a change in one degree in the acceptance angle can contribute up to a factor of 2 in the electron-capture cross section for angles between 2.3° and 3.5° depending on E.

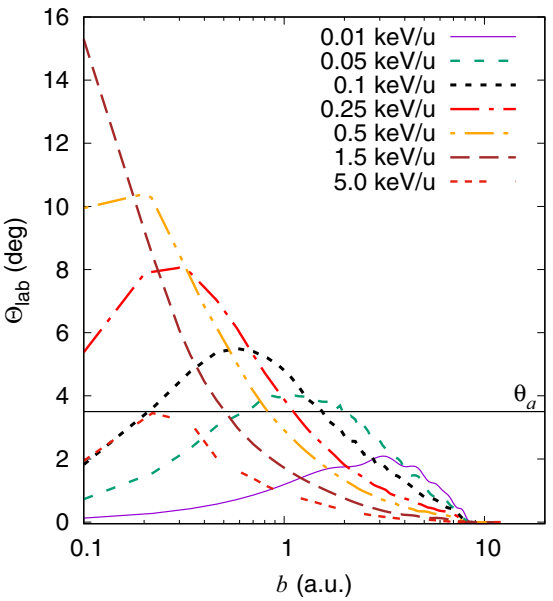

FIG. 5. Scattering angle in the laboratory frame, for use in Eq. (10) in the merged-beams configuration for the H^+ ions as a function of the impact parameter for relative collision energy per unit mass, $E = 0.01$, 0.05, 0.1, 0.25, 0.5, 1.5, and 5.0 keV/u. The horizontal line is the acceptance angle $\theta_a = 3.5°$ corresponding to our experimental system.

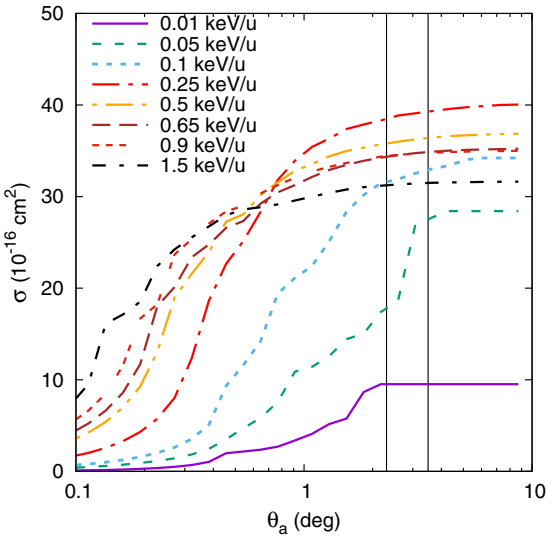

FIG. 6. Charge-transfer cross section as a function of the H^+ ions acceptance angle θ_a for C^{4+} colliding with H. The results are shown for E of 0.01, 0.05, 0.1, 0.25, 0.5, 0.6, 0.9, and 1.5 keV/u. The two vertical lines represent the acceptance angles of 2.3° and 3.5°. Note the influence of θ_a at low to intermediate values of E.

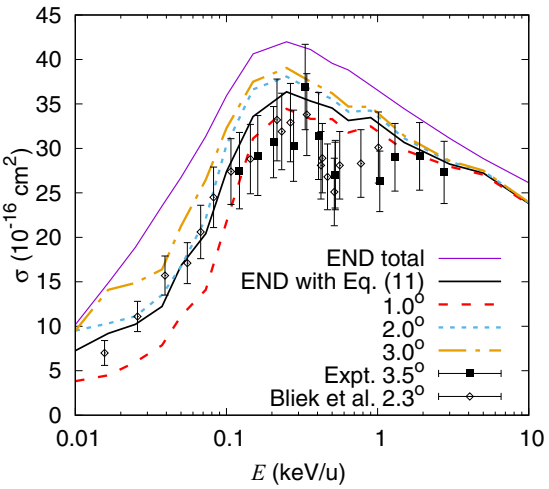

FIG. 7. Charge-transfer cross section when accounting for the effects of the merged-beams average over the path acceptance angle. The black solid thick line is the result of Eq. (11). The red long-dashed line is the result for only $\theta_a = 1^\circ$; the light-blue short-dashed line is for $\theta_a = 2^\circ$; and the light-brown dot-long dashed line is for $\theta_a = 3^\circ$. The total charge-transfer cross section when considering all the angles is shown by the purple solid thin line. The experimental data are the same as in Fig. 1. See text for details.

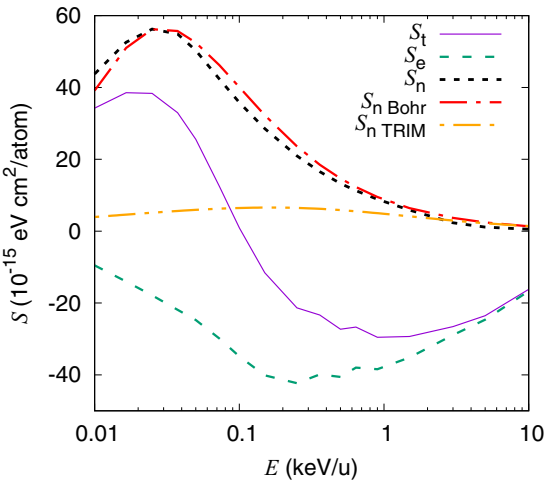

FIG. 8. Stopping cross section for C^{4+} colliding on atomic H as a function of E. Total projectile stopping cross section (purple solid line); electronic stopping cross section (green dashed line); nuclear stopping cross section (black short-dashed line); Bohr nuclear stopping cross section taking into account the high projectile charge (red dot-long-dashed line); and SRIM [34] nuclear stopping cross section for a neutral C colliding on atomic H (orange double-dot-dash line).

Furthermore, in the merged-beams experiment, the collision between the projectile and the target might occur at any point within the merged-beams path. Consequently, the scattering can occur with a different acceptance angle, depending on where the collision takes place along the merged-beams overlap region. To elucidate the consequences of this, the following simple assumptions (toy model) are considered. If $\rho(\theta_a)$ is the probability density for the collision to occur in a point of the merged-beams path with acceptance angle between θ_a and $\theta_a + d\theta_a$, then the averaged cross section over the acceptance angle along the merged-beams path is given by

$$\sigma = \int_{\theta_a^o}^{\theta_a^c} \rho(\theta_a)\sigma(\theta_a)d\theta_a\,, \tag{11}$$

where it is required that the probability per angle is normalized, i.e., $\int_{\theta_a^o}^{\theta_a^c} \rho(\theta_a)d\theta_a = 1$. Here θ_a^o is the acceptance angle for collisions occurring at the onset of the merged-beams overlap region and θ_a^c is the acceptance angle for collisions at the conclusion of the overlap region. By assuming that the collision occurs with the same probability at any point along the merged beam path, then the normalization condition requires that

$$\rho(\theta_a) = \frac{1}{\theta_a^c - \theta_a^o}\,. \tag{12}$$

In Fig. 7, we show the END results charge-transfer cross section when accounting for the values of the acceptance angle ranging from $\theta_a^o = 1.0^\circ$ to $\theta_c^c = 3.5^\circ$, which are geometrically deduced from a merged-beams path of 32.5 cm and an assuming an effective exit hole of ~ 1 cm. The black solid thick line is the result of Eq. (11) which accounts for the distribution of the collision along the merged-beams path. The red long-dashed line is the result for only $\theta_a = 1^\circ$; the light-blue short-dashed line is for $\theta_a = 2^\circ$; and the light-brown dot-long dashed line is for $\theta_a = 3^\circ$ [using Eq. (4)]. We compare our results to the case when all scattering angles are accounted for (purple solid thin line) as well as to the available ORNL merged-beams experimental data shown in Fig. 1. Interestingly, we note that the resemblance to the experimental data is much better (black solid thick line). In particular, our theoretical results show a similar structure observed at 0.5 keV/u, though somewhat broader. At lower values of E, the agreement with the experimental data is excellent. We conclude that the acceptance angle along the merged-beams path of the experimental set up strongly affects the collection of H^+ ions for this particular scattering system when the merged-beams path is accounted for.

E. Stopping cross section

To gain a further understanding of the results for the electron-capture cross section, we calculate the stopping cross section as the charge-transfer process is completely correlated to the energy loss process [33].

In Fig. 1, we show the projectile energy loss, $\Delta\mathcal{E}$, weighted by the impact parameter, as a function of the impact parameter for C^{4+} colliding on atomic H. For $E \lesssim 0.2$ keV/u and impact parameters $b < 3$ a.u., we find that the projectile loses kinetic energy when it collides with atomic H. Conversely, there is a small region of energy gain for $4 < b < 8$ a.u. For E around the maximum of the electron-capture cross section 0.5 keV/u, we observe that there is a larger energy gain, i.e., the projectile is accelerated, particularly for impact parameters between $3 < b < 7$ a.u. Furthermore, the peak of the electron-capture probability coincides with the maximum energy gain of the projectile and with a similar trend towards high E, in agreement with previous findings and energy conservation [33].

In Fig. 8, we also show the stopping cross section for C^{4+} colliding on atomic H as a function of E. Interestingly, the maximum energy loss cross section occurs at low values of

E with a maximum around 0.02 keV/u, a region where the charge exchange has a small contribution. In this case, the large energy loss is produced by a large electronic polarization and excitations of the hydrogen electron. A second maximum occurs at high values of E, where the ionization process is the responsible channel. Between 0.1 and 10 keV/u, we observe that the projectile gains energy. At $E \approx 1$ keV/u, we have the largest energy gain in the projectile kinetic energy, that is, the projectile is accelerated (exoergic collision). For $E \gtrsim 1$ keV/u, we note that the projectile still gains energy, but at a lower rate, as the ionization channel starts to open. Consequently, the behavior in the electron-capture cross section observed between 0.5 and 1 keV/u correlates strongly to the kinetic energy gain of the projectile.

Furthermore, in Fig. 8, we show the target displacement energy gain (nuclear stopping cross section S_n) for the hydrogen target (black short-dashed line). The maximum nuclear energy gain by the target recoil occurs around 0.03 keV/u. The orange double-dot-dashed line is the nuclear stopping cross section as obtained for a neutral carbon atom colliding with atomic H from the SRIM code [34], which is smaller than our results and is shown for comparison. However, by taking into account the high projectile charge, $Z_p = q = 4$, we can calculate S_n from Bohr theory [35], which shows a very good agreement with our END results (red dot-long-dashed line). As shown by Eq. (5), the remaining energy goes into the electronic excitations of the system. In Fig. 8, we show the electronic stopping cross section noticing that for E between 0.1 and 10 keV/u the collision is completely exoergic showing a negative electronic stopping cross section (projectile acceleration). This behavior results mainly from the energetics of the capture by the C^{4+} ion with a gain of kinetic energy by the projectile, as described above. Furthermore, the maximum in the electronic energy loss coincides with the peak of the electron-capture cross section.

V. CONCLUSION

We report a theoretical and experimental study of absolute cross sections for the charge-transfer process for collisions of C^{4+} with atomic hydrogen. We find reasonable agreement with previous merged-beams studies [8], as well as with measurements performed using different techniques [4,6]. By means of an electron-nuclear dynamics approach, we find that the 3ℓ states are the dominant electron-capture channel, and are, in part, responsible for the experimentally observed peak around $E \approx 0.5$ keV/u. For the energy dependence of the cross section, we also find good agreement with summed state-selective relative measurements [7]. We elucidate that the observed structure around the maximum of the electron-transfer cross section results, partly, by accounting for the merged-beams acceptance angle of the experiment along the collision path. We also find that the observed behavior in the capture cross section is the result of the electron-nuclei coupling with an energy gain in the projectile kinetic energy for relative collision energies between 0.1 and 10 keV/u, showing a correspondence with the charge-exchange impact-parameter-dependent probability due to the exoergecity of the collision. For the energy dependence of the cross section, we also find good agreement with summed state-selective relative measurements [7].

ACKNOWLEDGMENTS

We thank C. C. Havener for enabling our use of the ion-atom merged-beams apparatus at ORNL and for stimulating discussions. Work performed at ORNL was supported, in part, by the Division of Chemical Sciences, Office of Basic Energy Sciences, and the Division of Applied Plasma Physics, Office of Fusion Energy Sciences, US Department of Energy under Contract No. DE-AC05-00OR22725 with UT-Battelle, LLC. H.B. and D.W.S. were supported, in part, by NSF Stellar Astronomy and Astrophysics Grant No. AST-0606960 and by NASA Astronomy and Physics Research and Analysis Grant No. NNG06WC11G. H.B. was also supported, in part, by the German Academic Exchange Service DAAD. R.C.T acknowledges support from grants UNAM-DGAPA-PAPIIT IN-111-820 and LANCAD-UNAM-DGTIC-228 as well as to the University of Heidelberg for its hospitality.

[1] G. J. Ferland, K. T. Korista, D. A. Verner, and A. Dalgarno, Astrophys. J., Lett. **481**, L115 (1997).
[2] P. Gohil, K. H. Burrell, R. J. Groebner, K. Holtrop, D. H. Kaplan, and P. Monier-Garbet, Rev. Sci. Instrum. **70**, 878 (1999).
[3] B. Bransden, E. Bransden, M. McDowell, and M. McDowell, *Charge Exchange and the Theory of Ion-Atom Collisions*, International series of monographs on physics, (Clarendon, New York, 1992).
[4] R. A. Phaneuf, I. Alvarez, F. W. Meyer, and D. H. Crandall, Phys. Rev. A **26**, 1892 (1982).
[5] D. Ciric, D. Dijkkamp, E. Vlieg, and F. J. de Heer, J. Phys. B: At. Mol. Phys. **18**, L17 (1985).
[6] D. Dijkkamp, D. Ciric, E. Vileg, A. de Boer, and F. J. de Heer, J. Phys. B: At. Mol. Phys. **18**, 4763 (1985).
[7] R. Hoekstra, J. P. M. Beijers, A. R. Schlatmann, R. Morgenstern, and F. J. de Heer, Phys. Rev. A **41**, 4800 (1990).
[8] F. W. Bliek, R. Hoekstra, M. E. Bannister, and C. C. Havener, Phys. Rev. A **56**, 426 (1997).
[9] W. Fritsch and C. D. Lin, J. Phys. B: At. Mol. Phys. **17**, 3271 (1984).
[10] M. Gargaud and R. McCarroll, J. Phys. B: At. Mol. Phys. **18**, 463 (1985).
[11] M. Gargaud, R. McCarroll, and P. Valiron, J. Phys. B: At. Mol. Phys. **20**, 1555 (1987).
[12] H. C. Tseng and C. D. Lin, Phys. Rev. A **58**, 1966 (1998).
[13] L. F. Errea, J. D. Gorfinkiel, C. Harel, H. Jouin, A. Macías, L. Méndez, B. Pons, and A. Riera, J. Phys. B: At., Mol. Opt. Phys. **32**, L673 (1999).
[14] N. Vaeck, M. Desouter-Lecomte, and J. Liévin, J. Phys. B: At., Mol. Opt. Phys. **32**, 409 (1999).
[15] C.-N. Liu, A.-T. Le, and C. D. Lin, Phys. Rev. A **68**, 062702 (2003).

[16] C. Havener, E. Galutschek, R. Rejoub, and D. Seely, Nucl. Instrum. Meth. B **261**, 129 (2007).
[17] E. Deumens, A. Diz, R. Longo, and Y. Öhrn, Rev. Mod. Phys. **66**, 917 (1994).
[18] E. Deumens, T. Helgaker, A. Diz, H. Taylor, J. Oreiro, B. Mogensen, J. A. Morales, M. C. Neto, R. Cabrera-Trujillo, and D. Jacquemin, *ENDyne version 2.8 Software for Electron Nuclear Dynamics*, Quantum Theory Project, University of Florida, Gainesville (2000).
[19] T. H. Dunning, J. Chem. Phys. **90**, 1007 (1989).
[20] R. C. Raffenetti, J. Chem. Phys. **59**, 5936 (1973).
[21] R. D. Bardo, Even-tempered Gaussian atomic orbital bases in quantum chemistry: ab initio calculations on atoms hydrogen through krypton and on molecules containing carbon, hydrogen, and oxygen, Master's thesis, Retrospective Theses and Dissertations, Iowa State University, 1973.
[22] R. Cabrera-Trujillo, Y. Öhrn, E. Deumens, and J. R. Sabin, J. Chem. Phys. **116**, 2783, 2002.
[23] N. Bohr, Mat. Fys. Medd. Dan. Vid. Selsk. **18**, no. 8 (1948).
[24] C. C. Havener, M. S. Huq, H. F. Krause, P. A. Schulz, and R. A. Phaneuf, Phys. Rev. A **39**, 1725 (1989).
[25] C. C. Havener, *Accelerator-Based Atomic Physics Techniques and Applications* (AIP, New York, 1997).
[26] D. Seely, H. Bruhns, D. Savin, T. Kvale, E. Galutschek, H. Aliabadi, and C. Havener, Nucl. Instrum. Meth. A **585**, 69 (2008).
[27] R. E. Olson and M. Kimura, J. Phys. B: At. Mol. Phys. **15**, 4231 (1982).
[28] C. C. Havener, R. Rejoub, P. S. Krstić, and A. C. H. Smith, Phys. Rev. A **71**, 042707 (2005).
[29] N. Stolterfoht, R. Cabrera-Trujillo, Y. Öhrn, E. Deumens, R. Hoekstra, and J. R. Sabin, Phys. Rev. Lett. **99**, 103201 (2007).
[30] G. W. F. Drake, G. A. Victor, and A. Dalgarno, Phys. Rev. **180**, 25 (1969).
[31] M. Druetta, S. Martin, and J. Desesquelles, Nucl. Instrum. Meth. B **23**, 268 (1987).
[32] P. Barragán, L. F. Errea, F. Guzmán, L. Méndez, I. Rabadán, and I. Ben-Itzhak, Phys. Rev. A **81**, 062712 (2010).
[33] R. Cabrera-Trujillo, J. R. Sabin, Y. Öhrn, and E. Deumens, Int. J. Quantum Chem. **94**, 215 (2003).
[34] J. F. Ziegler, J. P. Biersack, and U. Littmark, *The Stopping and Range of Ions in Solids* (Pergamon, New York, 1985).
[35] R. Cabrera-Trujillo, J. R. Sabin, Y. Ohrn, E. Deumens, and N. Stolterfoht, Phys. Rev. A **83**, 012715 (2011).